THE EFFECT OF FLOW-INDUCED ORIENTATION ON THE RHEOLOGY OF CARBON NANOFIBER/POLYSTYRENE COMPOSITES DURING FLOW REVERSAL EXPERIMENTS

Thesis

Presented in Partial Fulfillment of the Requirements for Graduation with Honors Research Distinction in the College of Engineering of The Ohio State University

By

William L. Murch, B.S.

Chemical and Biomolecular Engineering

The Ohio State University

2011

Thesis Committee:

Kurt W. Koelling, Advisor

David L. Tomasko

Abstract

The effects of carbon nanofiber orientation and flow history on the subsequent shear rheology of polystyrene/carbon nanofiber composites were studied using experimental measurements and constitutive modeling. Results from flow reversal experiments show that the pre-orientation of carbon nanofibers has a significant effect on the transient shear behavior, specifically on the characteristic stress overshoot. The mass fraction of carbon nanofibers has a significant effect on the rheology when the fibers are initially randomly oriented, but not necessarily when there is pre-orientation in the flow direction. In addition, the initial composite stress, controlled by using variable rest times between flow reversals, has a significant effect on the observed transient behavior. Experimental results are compared with a microstructurally-based constitutive model designed to predict the flow behavior and carbon nanofiber orientation. It is demonstrated that the model predicts the effects of particle orientation and flow history during flow reversal experiments.

Acknowledgements

I would like to sincerely thank my advisor, Dr. Kurt W. Koelling, for his guidance throughout my career at Ohio State. Dr. Koelling provided me with ample advice, but always allowed me the freedom to discover and learn on my own. I would like to thank my fellow undergraduate research partners in the lab, Joseph Janko and Lukas Brooks. I would like to thank Dr. Chris Kagarise for helping me get started in my research and graciously allowing me to continue on his research work. I would also like to thank Sunni Modi for his help in the lab. Finally, I would like to thank Dr. David Tomasko and Dr. James Rathman for their assistance with this research.

Vita

2007 ……..… Finneytown High School

2011 .....…… B.S. Chemical and Biomolecular Engineering, The Ohio State University

2011 to Current ……...…… Engineer, Whirlpool Corporation

Field of Study

Major Field: Chemical and Biomolecular Engineering

Table of Contents

Introduction 1

Experimental Procedures 4

Materials 4

Sample Preparation. 5

Rheological Characterization. 6

Modeling 6

Constitutive Model 7

Model Fitting. 12

Experimental Results 16

Oscillatory Shear. 16

Steady Shear. 17

Transient Shear Start-Up 18

Flow Reversal. 21

Conclusions and Future Work 30

List of Tables

Table 1: Giesekus Model Fitting Parameters Found from the Pure Polymer. 15

List of Figures

Figure 1: Model Fitting of the Parameters η and λ using SAOS Data. 13

Figure 2: Model Fitting of the Parameter α using Steady Shear Data. 14

Figure 3: Storage and Loss Moduli Curves from SAOS Frequency Sweeps. 17

Figure 4: Steady Shear Viscosity versus Shear Rate. 18

Figure 5: Transient Shear Viscosity Curves versus Time. 20

Figure 6: Stress Overshoot versus Shear Rate during Forward Transient Shear Experiments. 20

Figure 7: Transient Viscosity Response Curves during Flow Reversal at a Shear Rate of 1.0 s^{-1} for (a.) 0wt% (b.) 2wt%, and (c.) 5wt% Samples. 24

Figure 8: Transient Viscosity Response Curves during Flow Reversal for 5wt% Samples at Shear Rates of (a.) 0.1 s^{-1} (b.) and 0.01 s^{-1}. 26

Figure 9: Stress Overshoot versus Rest Time during Transient Reverse Shear Experiments. 28

Figure 10: Transient First Normal Stress Difference during Flow Reversal at a Shear Rate of 1.0 s^{-1} for (a.) 0wt% (b.) 2wt%, and (c.) 5wt% Samples. 29

Introduction

There has been a great deal of recent interest in the use of polymer nanocomposites due to their potentially enhanced mechanical, electrical, and thermal properties (Dyke and Tour, 2004; Geng *et al*., 2002; Ramasubramaniam *et al*., 2003; Biercuk *et al*., 2002; Choi *et al*., 2003; Du *et al*., 2006; Yang *et al*., 2005). Nanoparticles are especially attractive due to their ability to produce enhanced properties in composites at lower particle loadings compared to traditional fillers, such as carbon black, glass fiber, and carbon fiber (Jaing *et al*., 2005; Mencke *et al*., 2004). This is fundamentally attributable to the greater surface area-to-volume ratio of nanoparticles compared to their micro-scale counterparts. In addition to aspect ratio and weight percent, the orientation of anisotropic nanoparticles in the polymer matrix strongly affects the resulting performance properties of the composite (Miyazono *et al.*, 2011). To understand how the processing of these composites will affect their properties, it is first critical to predict the flow-induced orientation and understand its effect on the subsequent rheology.

Much of the initial research into carbon nanoparticles was invested into single-walled nanotubes (SWNTs), following their discovery in the early 1990s (Iijima, 1991). However, due to their high cost, the use of SWNTs in commercial products has to this point been cost-prohibitive. Carbon nanofibers (CNFs) have been more recently studied as a low-cost alternative to nanotubes. CNFs are typically about 100 times larger in both length and diameter, but are up to 500 times less expensive (Wang *et al.*, 2006). The shear rheology of polymer/CNF composites has been studied previously in polycarbonate (Caldeira *et* al, 1998; Carneiro *et al.*, 1998; Hammel *et al.*, 2004; Higgins and Brittain, 2005), polyethylene (Lozano *et al.*, 2004), polypropylene (Hammel *et al.*, 2004; Tibbetts

and McHugh, 1999; Van Hattum *et al.*, 1999; Carneiro and Maia, 2000; Lozano and Barrera, 2001; Lozano *et al.*, 2001; Ceccia *et al.*, 2008; Kumar *et al.*, 2002), polyester (Ma *et al.*, 2003), polyamide (Tibbetts and McHugh, 1999; Lake *et al.*, 2002), polyimide (Glasgow *et al.*, 2004), poly(methyl methacrylate) (Cooper *et al.*, 2002; Zeng *et al.*, 2004), and polystyrene (Cipriano *et al.*, 2008) polymer matrices.

This particular study is performed on a polystyrene (PS) and carbon nanofiber composite. Previously, this group has investigated the shear and extensional rheology of similar PS/CNF composites (Xu *et al.*, 2005; Wang *et al.*, 2006; Miyazono *et al.*, 2011). Also from this group, a constitutive model was presented and validated against experimental results for both CNF (Wang *et al.*, 2006; Miyazono *et al.*, 2011) and nano-clay systems (Kagarise *et al.*, 2008). Most recently, a method was presented to quantitatively measure the flow-induced orientation of CNFs, allowing for comparisons with the model predictions during transient shear and extensional flows (Kagarise *et al.*, 2010, Kagarise *et al.*, 2011). The study here expands on the prior work of this group by looking at experimental results and model predictions of *flow reversal* experiments.

A flow reversal experiment consists of three distinct periods. Starting at rest, an initially randomly-oriented sample is sheared in the "forward" direction for a given strain until a steady-state is reached. Shear flow is then switched off, allowing the sample to relax for a given rest time. Shear flow is induced in the "reverse" direction on this flow-oriented sample until steady-state is again reached, after which the flow is ceased. Flow reversal experiments are thus studies of both the linear and nonlinear rheology of materials, and allow for the stress growth during start-up and stress decay during relaxation to be investigated. The start-up periods often exhibit stress overshoots for

composite materials, indicative of the stretching and rearrangement of polymer molecules as well as the orientation of the nanoparticles. By studying the stress overshoots and normal differences during start-up, conclusions regarding the particle orientation and structure build-up can be formed. Different rest times during the relaxation periods result in different amounts of recovery of the composite structure, which are then observed by the degree of stress overshoot during the reverse flow period (Eslami *et al.*, 2009). Flow reversal studies have been performed on polypropylene/nanoclay composites (Solomon *et al.*, 2001; Letwimolnun *et al.*, 2007) and PBSA/nanoclay composites (Eslami *et al.*, 2009). This research group presented limited results of flow reversal studies on a PS/CNF composite as part of a broader study (Kagarise *et al.*, 2010), although these results focused only on the effect of the rest time and were not validated using any modeling techniques. This study did, however, provide the basis for interest in further research into the effect of flow history.

This paper first presents the materials, sample preparation, and rheological characterization methods used in this study. A modified version of the constitutive model previously presented by this group (Wang *et al.*, 2006; Kagarise *et al.*, 2008; Kagarise *et al.*, 2010; Kagarise *et al.*, 2011) is then reviewed and discussed. This modeling section will focus on the fitting of the model to this system and the changes made to the previously presented model that allow for the modeling of flow reversal experiments and the quantification of normal forces. The experimental results are then discussed, with the focus on transient shear flows in the forward and reverse directions. In this results section, these experimental results will be compared thoroughly to modeling predictions.

The variables investigated in this experiment were CNF weight percent, shear rate, and rest time. The effects of these variables were investigated, both experimentally and from model predictions, by studying the shear stress and first normal difference during the periods of flow start-up, steady-state, and relaxation. The scope of this paper did not include the quantitative measurement of the CNF orientation using microscopy techniques, presented previously by this group (Kagarise *et al.*, 2011). Instead, the focus of this paper was directed towards the description of experimentally observed phenomena and the validation of model predictions. The final section in this paper will discuss conclusions of the research and recommendations for future work.

Experimental Procedures

Materials. The polystyrene used in this study was supplied by the Chevron Phillips Chemical Co. LP (MC3600). The PS has a specific gravity of 1.03 and a melt flow rate of 13.0 g/10 min (200°C/5 kg, method: ASTM D1238). Polystyrene was chosen as the thermoplastic polymer matrix in this study because its rheology has been well characterized, so any deviation caused by the addition of CNFs can be readily identified. Furthermore, its molecular structure is simple, with no crystalline structure present in the solid phase, allowing for the nanostructure of CNFs developed during flow in its molten phase to be preserved when the composite is cooled to the solid phase.

The CNFs used in this study were Pyrograf III (type PR-24-XT-HHT), manufactured by Applied Sciences, Inc, and used as-received. These CNFs are produced by decomposing organic vapors at elevated temperature in the presence of metal

catalysts, resulting in a nanofiber with a stacked-cup structure and a hollow core. This particular type of CNF (HHT) is high-heat treated to graphitize the fiber and remove more of the metal catalyst. The CNFs that were obtained were in a powder form, consisting largely of fiber agglomerates, most of which were less than 1 mm in diameter. These as-produced fibers had lengths of approximately 50-200 μm and average diameters of 100 nm according to manufacturer estimates.

Sample Preparation. The carbon nanofibers were dispersed in the polymer matrix by feeding PS and CNFs into a DACA Instruments twin-screw microcompounder at 200°C with a screw rotation rate of 250 RPM and mixing for 4 minutes. Composites were made containing CNF concentrations of 2 and 5 wt%. From the microcompounder, the composite samples were extruded from a 2 mm die, and after cooling, were cut into ~2-3 mm long pellets. Pure PS without nanofibers underwent the same melt blending procedure in order to take into account any possible degradation (e.g. oxidation or polymer chain breaking) that may have occurred. The processing conditions used here were chosen to balance good dispersion of the nanofibers with limited degradation of the polymer.

The pellets formed from the melt blending procedure were compression molded using a hot press at 200°C into 25 mm diameter disks of 0.9-1.2 mm thickness to be used in shear flow tests. The pellets were placed into molds and allowed to melt for 15 minutes with no pressure applied. This melting period was then followed by a cycle of quickly compressing and decompressing the samples four consecutive times to eliminate air bubbles. Pressure was then reapplied and held for 10 minutes. After that, the heat to the press was turned off and the samples were allowed to cool to below 100°C, the glass

transition temperature of PS. Once cooled, the pressure was released and the samples were removed from the mold. The samples were placed in a vacuum oven at 70°C for at least 24 hours, and remained there until the time they were tested to prevent them from absorbing moisture or air from the atmosphere.

Rheological Characterization. Shear rheology of the melt composites was measured using a strain-controlled rheometer from TA Instruments (ARES LS2) with both a torque transducer (0.02-2000 g-cm) and a normal force transducer (2-2000 g). Parallel plates of 25 mm diameter were used for all shear measurements. The measurement temperature was 160°C and the gap distance was kept in the range of 0.9-1.2 mm for all tests. Before testing began, the molded disks were allowed to rest at the measurement temperature of 160°C for 15 minutes in order to relax any residual stress introduced by the compression molding process and so the polymer could reach thermal equilibrium with the surroundings. With this rheometer, small amplitude oscillatory shear, steady shear, and transient shear experiments were performed.

Modeling

In this section, a constitutive model is presented for the prediction of the rheological behavior of PS/CNF composites. This model has been validated against experimental results in steady shear and shear start-up flows for PS/CNF composites (Wang *et al.*, 2006; Kagarise *et al.*, 2010) and for similar PS/nanoclay systems (Kagarise *et al.*, 2008). Model predictions have also been compared to extensional as well as shear flow results and flow-induced CNF orientation measurements (Kagarise *et al.*, 2011).

The model was modified in this study to predict the shear flow behavior, including the composite shear stress and normal force differences, during flow reversal experiments.

Constitutive Model. The constitutive model contains the following four governing equations [Eq. (1)-(4)]. These four equations are used to find the total composite stress [Eq. (1)], including the polymer stress [Eq. (2)] and the CNF stress [Eq. (3)], and the CNF orientation [Eq. (4)]:

$$\tau_{ij}^{c} = -p\delta_{ij} + 2\eta_s D_{ij} + \tau_{ij}^{p} + \tau_{ij}^{CNF}, \tag{1}$$

$$\sigma\tau_{ij,m}^{p} + \lambda_m \frac{D\tau_{ij,m}^{p}}{Dt} + \frac{\alpha_m\lambda_m}{\eta_{p,m}}\left(\tau_{ik,m}^{p}\tau_{kj,m}^{p}\right) + \frac{3(1-\sigma)}{2}\left(a_{ik}\tau_{kj}^{p} + \tau_{ik}^{p}a_{kj}\right) = 2\eta_{p,m}D_{ij}, \tag{2}$$

$$\tau_{ij}^{CNF} = 2[\eta_s + \eta]\phi\left[AD_{kl}a_{ijkl} + B\left(D_{ik}a_{kj} + a_{ik}D_{kj}\right) + CD_{ij} + 2Fa_{ij}D_r\right], \tag{3}$$

$$\frac{da_{ij}}{dt} = \left(W_{ik}a_{kj} - a_{ik}W_{kj}\right) + \chi\left(D_{ik}a_{kj} + a_{ik}D_{kj} - 2D_{kl}a_{ijkl}\right) + 4C_I\Pi_D^{\frac{1}{2}}(\delta_{ij} - 3a_{ij}). \tag{4}$$

The total composite stress is shown in Equation (1) (Azaiez, 1996). In this equation, the total stress is comprised of the pressure maintaining incompressibility, *p*, the stress from a Newtonian solvent, $2\eta_s D_{ij}$, the stress of the polymer, τ_{ij}^{p}, and the stress associated with the carbon nanofibers, τ_{ij}^{CNF}. In the term for the stress of the Newtonian solvent, D_{ij} is the symmetric part of the Eulerian velocity gradient, $\partial v_i/\partial x_i$, and η_s is the solvent viscosity. In this study, no solvent is present, so this solvent term is set to zero.

Equation (2) is the multi-mode Giesekus model (Bird *et al.*, 1987) which predicts the strain rate-dependent viscoelastic behavior of the polymer matrix. The total polymer stress is a summation of the polymer stress of all *N* modes:

$$\tau_{ij}^{p} = \sum_{m=1}^{N} \tau_{ij,m}^{p}. \quad (5)$$

The upper convected time derivative of τ_{ij}^{p} is

$$\frac{D\tau_{ij}^{p}}{Dt} = \frac{d}{dt}\tau_{ij}^{p} - W_{ik}\tau_{kj}^{p} + \tau_{ik}^{p}W_{kj} - D_{ik}\tau_{kj}^{p} - \tau_{ik}^{p}D_{kj}. \quad (6)$$

Where W_{ij} is the skew portion of the Eulerian velocity gradient. For shear flows,

$$D_{ij} = \begin{bmatrix} 0 & \dot{\gamma}/2 & 0 \\ \dot{\gamma}/2 & 0 & 0 \\ 0 & 0 & 0 \end{bmatrix}, \text{ and } W_{ij} = \begin{bmatrix} 0 & \dot{\gamma}/2 & 0 \\ -\dot{\gamma}/2 & 0 & 0 \\ 0 & 0 & 0 \end{bmatrix}. \quad (7)$$

Also from Equation (2), the three fitting parameters η_p, λ, and α represent the polymer zero-shear viscosity, relaxation time, and mobility factor, respectively, for the melt-phase polymer matrix. These three parameters can be fit based on experiments done on the pure polymer, as discussed in the following Model Fitting section. The stress tensor is symmetric with six terms (τ_{11}, τ_{22}, τ_{33}, $\tau_{12} = \tau_{21}$, $\tau_{13} = \tau_{31}$, and $\tau_{23} = \tau_{32}$), only four of which are nonzero in shear flow (τ_{11}, τ_{22}, τ_{33}, and τ_{12}). To solve for the stress components during transient shear flow from Equation (2), four coupled non-linear differential equations must be solved simultaneously. The term σ is the polymer-particle interaction parameter, an experimentally fitted parameter.

The flow-induced stress associated with the presence of carbon nanofibers is described by Equation (3) (Tucker, 1991). The term η is the polymer viscosity, which is defined for shear flow as

$$\eta = \frac{\tau_{12}^{p}}{\dot{\gamma}}, \quad (8)$$

Where $\tau_{12}^{p}$is the polymer stress component in the 1-2 direction, which can be solved for using Equation (2), and $\dot{\gamma}$ is the shear rate. The term ϕ in Equation (3) is the volume fraction of the CNFs, which can be solved from the nanofiber mass fraction and density and the polymer density. The terms *A*, *B*, *C*, and *F* are nanoparticle shape factors that are functions of the volume fraction and aspect ratio ($r = L/D$) of the CNFs. Definitions for these shape factors have been proposed (Tucker, 1991; Dinh and Armstrong, 1984; Shaqfeh and Fredrickson, 1990) for different concentration regimes (dilute or semidilute), states of nanoparticle orientation (isotropic or aligned), and flow conditions (transient or steady state). These have been summarized and individually analyzed in previous works of this group (Kagarise *et al.*, 2010; Kagarise *et al.*, 2011). The PS/CNF system investigated in this study falls under the categories of semi-dilute and aligned. For semi-dilute aligned systems, the shape factors *B*, *C*, and *F* are equal to zero, and the only nonzero shape factor is *A*. Based on the previous work by this group, the shape factor in Equation (9) has been shown to provide the best fit for this PS/CNF system (Kagarise *et al.*, 2010; Kagarise *et al.*, 2011):

$$A = \frac{r^2}{3\ln(\frac{\pi}{\phi})} \tag{9}$$

The average aspect ratio, *r*, for similar melt-blended samples (prepared using the same procedure as in this experiment) was found using microscopy techniques to be $r = 33$, with average nanofiber lengths of approximately $L = 3.3\ \mu m$ (Kagarise *et al.*, 2010; Kagarise *et al.*, 2011). The term D_r is the rotary diffusivity due to Brownian motion, which is defined as $D_r = 2C_I\Pi_D^{1/2}$. The parameter C_I is the hydrodynamic particle-particle interaction parameter, which quantifies the interactions between nanofibers and

their surrounding fibers, and Π_D is the second invariant of D_{ij}. The terms a_{ij} and a_{ijkl} are orientation tensors, which will be described next.

Equation (4) predicts the evolution of the carbon nanofibers in the melt-phase polymer matrix during flow according to the second order orientation tensor a_{ij}. The concept of the orientation tensor is further expanded upon in previous works of this group (Kagarise *et al.*, 2010; Kagarise *et al.*, 2011), but was not focused upon in this study. Equation (4) contains the shape parameter χ, which is a function of the aspect ratio

$$\chi = \frac{r^2+1}{r^2-1}. \tag{10}$$

The fourth-order orientation tensor a_{ijkl} cannot be solved for directly and instead must be related to the second-order tensor a_{ij}, using a closure approximation. Popular closure approximations include a linear approximation [Equation (11)], which works better for randomly-aligned states, the quadratic approximation [Equation (12)], which works better for highly-aligned states, and the hybrid closure approximation [Equation (13)], which is a combination of the linear and quadratic approximations and works well across the range of orientations (Advani and Tucker, 1990). Previous work from this group has investigated all three closure approximations and shown that the hybrid closure approximation provides the best predictions for these PS/CNF systems (Wang *et al.*, 2006). The hybrid closure approximation, shown in Equation (13), was used in all calculations in this study.

$$\hat{a}_{ijkl} = -\frac{1}{35}\left(\delta_{ij}\delta_{kl} + \delta_{ik}\delta_{jl} + \delta_{il}\delta_{jk}\right) + \frac{1}{7}(a_{ij}\delta_{kl} + a_{ik}\delta_{jl} + a_{kl}\delta_{ij} + a_{jl}\delta_{ik} + a_{jk}\delta_{il} + a_{il}\delta_{jk}), \tag{11}$$

$$\tilde{a}_{ijkl} = a_{ij}a_{kl}, \tag{12}$$

$$a_{ijkl} = (1-f)\hat{a}_{ijkl} + f\tilde{a}_{ijkl}, \quad \text{with } f = 1 - 27\det(a_{ij}). \tag{13}$$

With the closure approximation, Equations (3) and (4) can then be solved. By solving for the four nonzero stress components using Equation (3), the transient shear viscosity and the normal stress differences of the composite can be found. The transient shear viscosity, first normal difference, and second normal difference for shear flows are shown in Equations (14), (15), and (16), respectively:

$$\eta_c^+ = \frac{\tau_{12}^c}{\dot{\gamma}} \tag{14}$$

$$N1 = \tau_{11}^c - \tau_{22}^c, \tag{15}$$

$$N2 = \tau_{22}^c - \tau_{33}^c. \tag{16}$$

With the proper values of the shape factors and the closure approximation, the equations for the composite stress components, from Equation (3), are shown in Equations (17) through (20):

$$\tau_{12}^c = 2\eta\phi\left[A\dot{\gamma}\left[\begin{matrix}(27a_{11}a_{22}a_{33} - 27a_{33}a_{12}^2)\left(-\frac{1}{35} + \frac{(a_{11}+a_{22})}{7}\right) \\ +(a_{12}^2)(1 - 27a_{11}a_{22}a_{33} + 27a_{33}a_{12}^2)\end{matrix}\right]\right] \tag{17}$$

$$\tau_{11}^c = 2\eta\phi\left[A\dot{\gamma}\left[(27a_{11}a_{22}a_{33} - 27a_{33}a_{12}^2)\left(\frac{3a_{12}}{7}\right) + (a_{11}a_{12})(1 - 27a_{11}a_{22}a_{33} + 27a_{33}a_{12}^2)\right]\right] \tag{18}$$

$$\tau_{22}^c = 2\eta\phi\left[A\dot{\gamma}\left[(27a_{11}a_{22}a_{33} - 27a_{33}a_{12}^2)\left(\frac{3a_{12}}{7}\right) + (a_{22}a_{12})(1 - 27a_{11}a_{22}a_{33} + 27a_{33}a_{12}^2)\right]\right] \tag{19}$$

$$\tau_{33}^c = \left(2\eta\phi\left[A\dot{\gamma}\left[(27a_{11}a_{22}a_{33} - 27a_{33}a_{12}^2)\left(\frac{a_{12}}{7}\right) + (a_{33}a_{12})(1 - 27a_{11}a_{22}a_{33} + 27a_{33}a_{12}^2)\right]\right]\right) \tag{20}$$

The model presented here works for forward or reverse shear flows, for any real shear rate value, including zero (to model a rest period). In order to predict behavior

during flow-reversal experiments, this model had to allow for initial conditions to be input for the stress components and the CNF orientation, based on flow history. The model thus was modified to simulate sequential periods of forward and reverse shear flows, separated by rest periods, with the final stress and orientation values of one flow period used as the initial conditions for the following period.

Model Fitting. In order to use the constitutive model for this particular PS/CNF system, the values of the model fitting parameters had to be determined. These model fitting parameters include three parameters for the pure polymer, namely η_p, λ, and α, which represent the polymer zero-shear viscosity, relaxation time, and mobility factor, respectively, for the melt-phase polymer matrix. These parameters must be fit for each mode of the Giesekus model. For this PS/CNF system, it was determined that the least amount of polymer modes necessary to provide an adequate model was $N = 5$ modes, so a five-mode model was used in this study. The values for η_p and λ were found by fitting the equations

$$G'(\omega) = \sum_{m=1}^{N} \left(\frac{\eta_{p,m} \lambda_m \omega^2}{1+(\lambda_m \omega)^2} \right), \tag{21}$$

$$G''(\omega) = \sum_{m=1}^{N} \left(\frac{\eta_{p,m} \omega}{1+(\lambda_m \omega)^2} \right), \tag{22}$$

To experimentally measured small amplitude oscillatory shear (SAOS) values from the pure polymer, and minimizing the following error equation:

$$E_{SAOS} = \sum_{i=1}^{N} \left\{ \left[\log_{10} G'_{exp}(\omega_i) - \log_{10} G'(\omega_i) \right]^2 + \left[\log_{10} G''_{exp}(\omega_i) - \log_{10} G''(\omega_i) \right]^2 \right\}, \tag{23}$$

Where $G'_{exp}(\omega_i)$ and $G''_{exp}(\omega_i)$ are the experimentally measured values of the storage and loss moduli, and $G'(\omega_i)$ and $G''(\omega_i)$ are the model predictions according to Equations (21) and (22). Figure 1 shows the fitting of the model to the small amplitude oscillatory shear data.

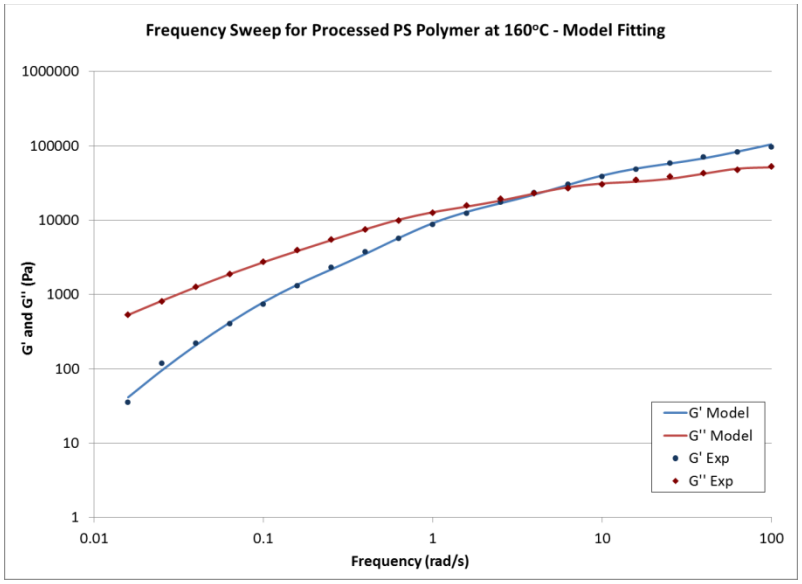

Figure 1: Model Fitting of the Parameters η and λ using SAOS Data.

The mobility factor, α, was determined by fitting the following equations

$$\eta(\dot{\gamma}) = \sum_{m=1}^{N} \left(\eta_{p,m} \frac{(1-f_m)^2}{1+(1-2\alpha_m)f_m} \right), \tag{24}$$

$$\psi_1 = 2\eta_{p,m}\lambda_m \left[\frac{f_m(1-\alpha_m f_m)}{(\lambda_m \dot{\gamma})^2 \alpha_m (1-f_m)} \right] \tag{25}$$

$$f_m = \frac{1-g_m}{1+(1-2\alpha_m)g_m}, \tag{26}$$

$$g_m = \sqrt{\frac{[1+16\alpha_m(1-\alpha_m)(\dot{\gamma}\lambda_m)^2]^{1/2}-1}{8\alpha_m(1-\alpha_m)(\dot{\gamma}\lambda_m)^2}}, \tag{27}$$

Where $\eta(\dot{\gamma})$is the steady-state shear viscosity, $\psi_1(\dot{\gamma})$ is the first normal force ($\psi_1 = N1/\dot{\gamma}^2$), and f_m and g_m are arbitrary variables.

These equations were fit to experimentally measured steady-state shear viscosity and first normal force values from the pure polymer, and minimizing the following equation:

$$E_{SS} = \sum_{i=1}^{N} \left\{ \left[\log_{10} \eta_{exp}(\dot{\gamma}_i) - \log_{10} \eta(\dot{\gamma}_i) \right]^2 + \left[\log_{10} \psi_{1,exp}(\dot{\gamma}_i) - \log_{10} \psi_1(\dot{\gamma}_i) \right]^2 \right\} \quad (28)$$

Where $\eta_{exp}(\dot{\gamma}_i)$ and $\psi_{1,exp}(\dot{\gamma}_i)$ are the experimentally measured values for the steady shear viscosity and the first normal force, and $\eta(\dot{\gamma}_i)$ and $\psi_1(\dot{\gamma}_i)$ are the model predictions according to Equations (24) and (25). Figure 2 shows the fitting of the model to the small amplitude oscillatory shear data.

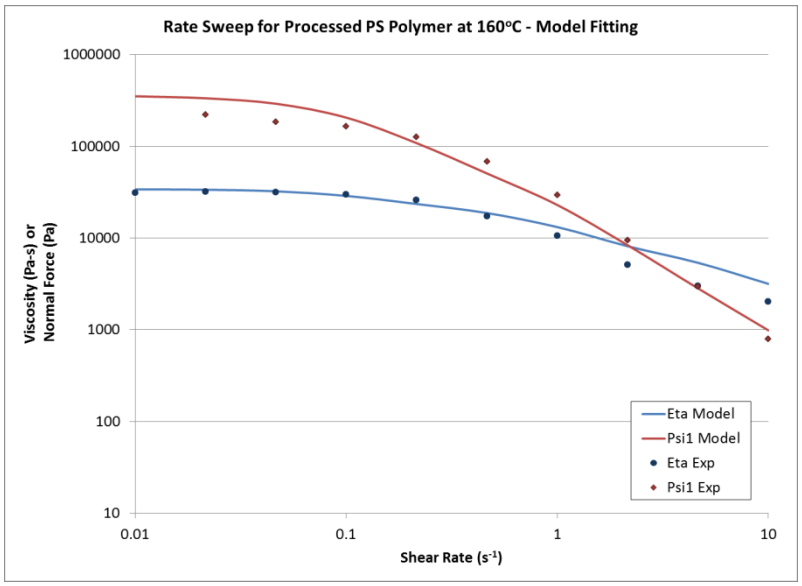

Figure 2: Model Fitting of the Parameter α using Steady Shear Data.

The complete list of Giesekus model parameters fit to the pure polymer for η_p, λ, and α are shown in Table 1.

Table 1: Giesekus Model Fitting Parameters Found from the Pure Polymer.

Mode	η_m	λ_m	α_m
1	982.013	0.0102478	0.747591
2	4771.59	0.117533	0.998137
3	13793.8	1.00233	0.999966
4	11048.3	7.17120	0.999995
5	3443.56	23.8926	0.0803719

The other model fitting parameter which must be found experimentally is C_I, the hydrodynamic particle-particle interaction parameter. The particle-particle interaction parameter greatly affects the predictions for the evolution of the CNFs during flow and the final steady-state alignment that can be achieved. Based on this understanding, experimental measurements of the final CNF alignment following an extended flow period can be compared to model predictions to calculate an optimal value for C_I. The final CNF alignment can be quantified using a microscopy technique outlined previously by this group (Kagarise *et al.*, 2011). Measurement of the CNF orientation was not the focus of this study, so the previously calculated value $C_I = 0.031$, measured from shear flow experiments (Kagarise, 2009), is used in all model predictions presented here.

The polymer-particle interaction parameter, σ, has been shown to be equal to one based on experimental results (Kagarise, 2009). This greatly simplifies Equation (2), essentially resulting in the assumption that there is no effect of carbon nanofiber orientation on the polymer stress. By changing this value to a number less than one, it would make the polymer stress a function of the CNF orientation, likely making a significant difference on the model predictions. Whether the assumption of $\sigma = 1$ is

valid or not is a critical debate, but it is not the focus of this study. Instead, it will be considered in future works, as described in the Conclusions and Future Work section.

Experimental Results

This section contains the results of the rheological experiments that were performed on this PS/CNF system. First, results of small amplitude oscillatory shear tests are presented, followed by tests performed at steady shear. Next is the discussion of transient shear start-up experiments, and finally the results of flow reversal studies. Each set of results is compared and validated against model predictions.

Oscillatory Shear. The small amplitude oscillatory shear response of a sample was measured across a range of frequencies to find the storage $G'(\omega)$ and loss $G''(\omega)$ moduli curves. These are shown for the three different CNF loadings in Figure 3. As this figure shows, the storage and loss moduli increased with increasing CNF loadings. This result matches the trend found for polypropylene/CNF composites (Lozano *et al.*, 2001). An increase in both moduli gives an indirect indication that the strength of the material has increased.

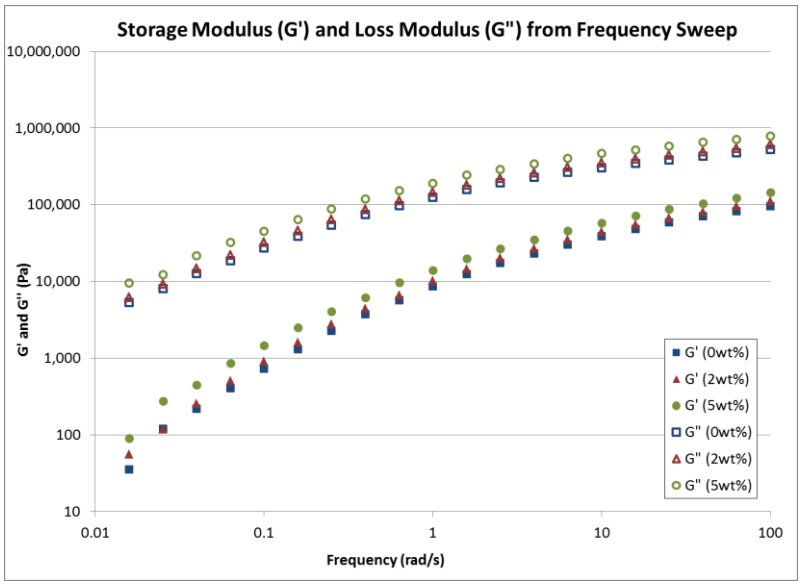

Figure 3: Storage and Loss Moduli Curves from SAOS Frequency Sweeps. The loss modulus curve has been multiplied by a factor of 10^1 for clarity of results.

Steady Shear. Steady shear experiments were run for the three different CNF loadings at the three shear rates investigated in this study. These steady shear values were recorded from the final values of transient tests, which are described in the next section, after the sample was believed to have reached steady state. These results were then compared to model predictions across the range of shear rate values, shown in Figure 4.

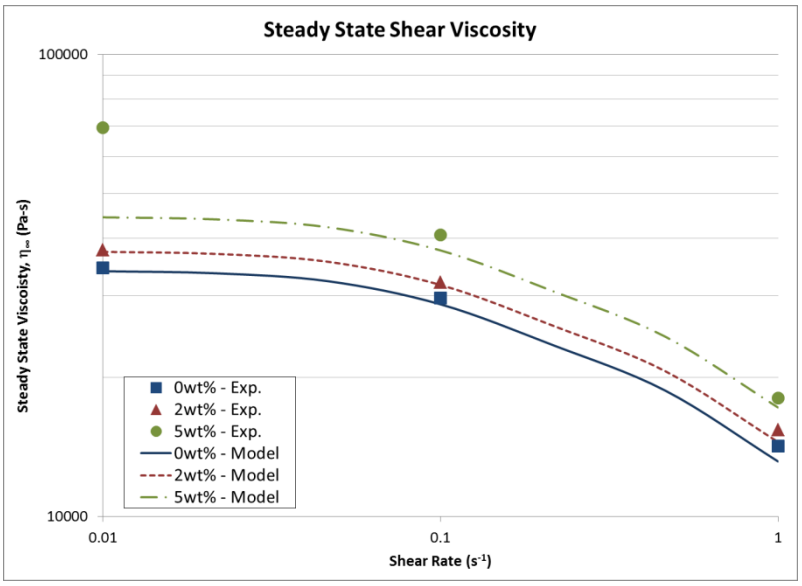

Figure 4: Steady Shear Viscosity versus Shear Rate.

The experimental steady shear viscosity values match very well to the model predictions, especially at the shear rates above $\dot{\gamma} = 0.01\ s^{-1}$. Both the experimental results and model predictions show general shear-thinning behavior (decreasing steady shear viscosity as shear rate increases) across this range of shear rates. The only experimental point that deviates significantly from the model prediction curve is for the 5wt% sample at a shear rate of $\dot{\gamma} = 0.01\ s^{-1}$. As described further in the following results section, the results of shear testing at the lowest shear rate, $\dot{\gamma} = 0.01\ s^{-1}$, did not show the same trends that were exhibited during testing at higher shear rates.

Transient Shear Start-Up. Transient shear tests measure the rheological response of a sample during the start-up period of shear flow until the sample has reached a steady shear state. Transient shear results of polymer melts typically show an initial sharp rise in shear stress, followed by a stress maximum, or overshoot, being reached. The shear stress then decreases to a constant nonzero steady state value.

The characteristic stress overshoot can be visualized by considering how polymer melts are modeled using the Giesekus model. Individual polymer molecules are approximated as two rigid spheres, connected by an ideal Hookean spring. As these randomly oriented polymer molecules undergo a shear flow, the two rigid spheres are located at different points across the velocity gradient, thus undergoing different forces, and stretching the spring. The spring is stretched until the rigid spheres become approximately aligned in the direction of shear flow, upon which the spring will relax slightly. This initial stretching and subsequent partial relaxation of the elastic polymer chains as they become flow-aligned results in the observed stress overshoot.

The transient shear viscosity for different samples at two shear rates can be observed in Figure 5. The stress overshoot, described previously, can be seen clearly in this figure, as shear viscosity is directly proportional to shear stress [Equation (14)]. As the CNF weight percent increases, so does the magnitude of the overshoot. As the shear rate increases, the overshoot occurs at a later time – however, note that the overshoot occurs for all trials at a strain ($\gamma = \dot{\gamma} t$) of approximately $\gamma = 1$. As the CNF weight percent increases and the shear rate decreases, the viscosity curves reach higher steady state values, trends supported in the previous section (Figure 4).

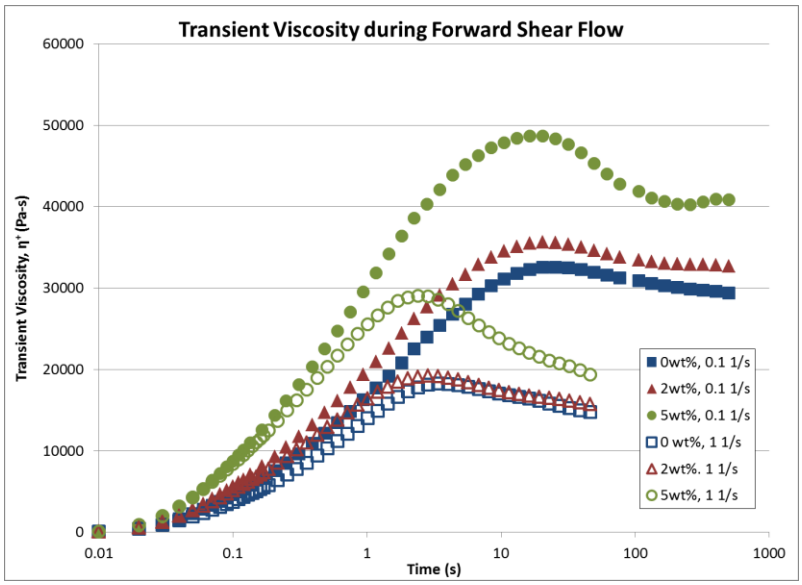

Figure 5: Transient Shear Viscosity Curves versus Time.

The stress overshoot can be quantified by finding the ratio of the maximum stress value to the steady shear stress value. Figure 6 displays the experimentally measurements and model prediction curves for the stress overshoot experienced during transient shear flows.

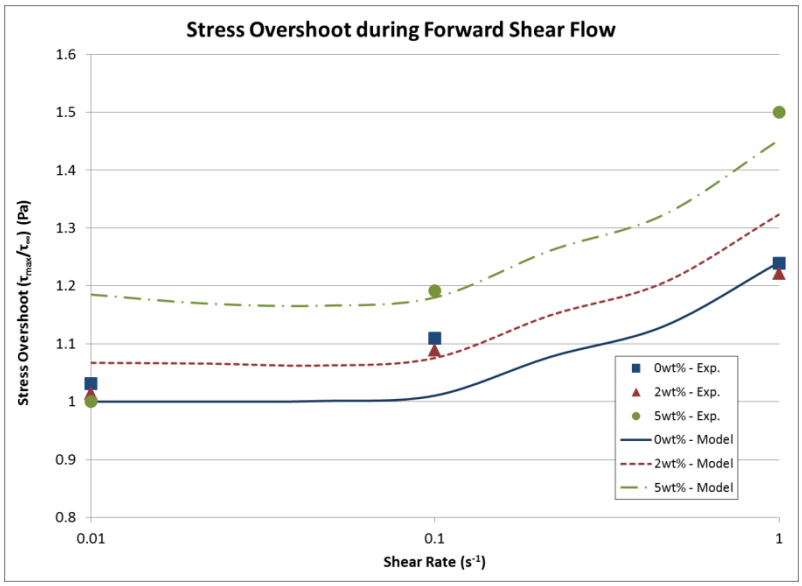

Figure 6: Stress Overshoot versus Shear Rate during Forward Transient Shear Experiments.

The model predicts that the stress overshoot value should increase at increasing CNF loadings and increasing shear rates. The trend of increasing stress overshoot is observed experimentally at increasing shear rates. The increasing overshoot trend is not as clear at increasing CNF loadings, although it is generally still apparent, especially at the higher shear rates.

Flow Reversal. Flow reversal experiments were performed using three flow period trials. The first period consisted of shear in the forward (clock-wise) direction. This was following by a rest period of a certain time length. Finally, the sample was sheared in the reverse (counter clock-wise) direction. The shear stress and first normal force difference were measured during each flow and rest time period, and are compared to model predictions in this section. Flow reversal experiments were run at three CNF weight percents (0wt%, 2wt%, and 5wt%), three shear rates (0.01 s^{-1}, 0.1 s^{-1}, and 1.0 s^{-1}), and three rest times. All flow periods were run for constant strains of $\gamma = 50$, with the flow time related inversely to the shear rate for each trial.

These rest times were chosen to capture three states of the polymer composite before flow resumed: no polymer relaxation (a rest time of zero), partial polymer relaxation, and complete polymer relaxation. From Table 1 in the Modeling section, it was shown that the longest model-fitted relaxation time, for mode five, is approximately 24 seconds. Thus, it was conjectured that the two nonzero rest times should be chosen on either side of this longest relaxation time. The three rest times that were ultimately chosen for this experiment were t_{rest} = *0, 20,* and *400 s.*

The transient viscosity curves for flow reversal studies performed at a shear rate of $\dot{\gamma} = 1.0\ s^{-1}$ are displayed in Figure 7. The three graphs for each weight percent are plotted on the same axes scales to allow for better comparison. For flow reversal studies on a pure polymer, it is expected that the forward shear direction will produce the characteristic overshoot, as seen in Figure 7a. For a rest time of $t_{rest} = 0\ s$, the reverse viscosity curve should exhibit a negligible overshoot, since no relaxation or rearrangement of polymer chains could've taken place between flows. A relatively small overshoot was observed experimentally in Figure 7a for a rest time of $t_{rest} = 0\ s$. As the rest time increases, it is expected that the reverse viscosity curve's overshoot will increase until at a long enough rest time, the polymer will be completely relaxed. In the limit of complete polymer relaxation, the forward and reverse viscosity curves should overlay one another completely. This trend is seen qualitatively in the data, with the viscosity curves experiencing larger overshoots as the rest time increases. The forward and reverse curves should reach the same steady shear viscosity value, assuming no permanent changes have been made to the polymer microstructure; any deviation from this is indicative of experimental error.

For the polymer composites, certain trends are expected to be similar to those for the pure polymer. In general, as the rest time increases, so should the overshoot, as is observed in Figures 7b and 7c. However, instead of considering just the relaxation of the polymer chains during the rest period, the reorientation of CNF particles – and how they interact with one another and the polymer – must be considered in flow reversals of composites. An overshoot is expected for composite samples, even at a rest time of $t_{rest} = 0\ s$, illustrative of the reorientation of CNFs. In addition, the forward and reverse

viscosity curves will never overlay one another – even at an infinite rest time – since they begin at different states of CNF orientation. The forward flow begins with a randomly oriented sample, while the reverse flow begins with a sample with nanofibers already oriented in the direction of flow.

In general, the model predictions do well to capture the qualitative trends and the shapes of the transient viscosity curves. The model predictions do especially well at strains below the overshoot strain ($\gamma < 1$). Quantitatively, the model predictions still do an adequate job of estimating the values of the transient viscosity, within experimental error.

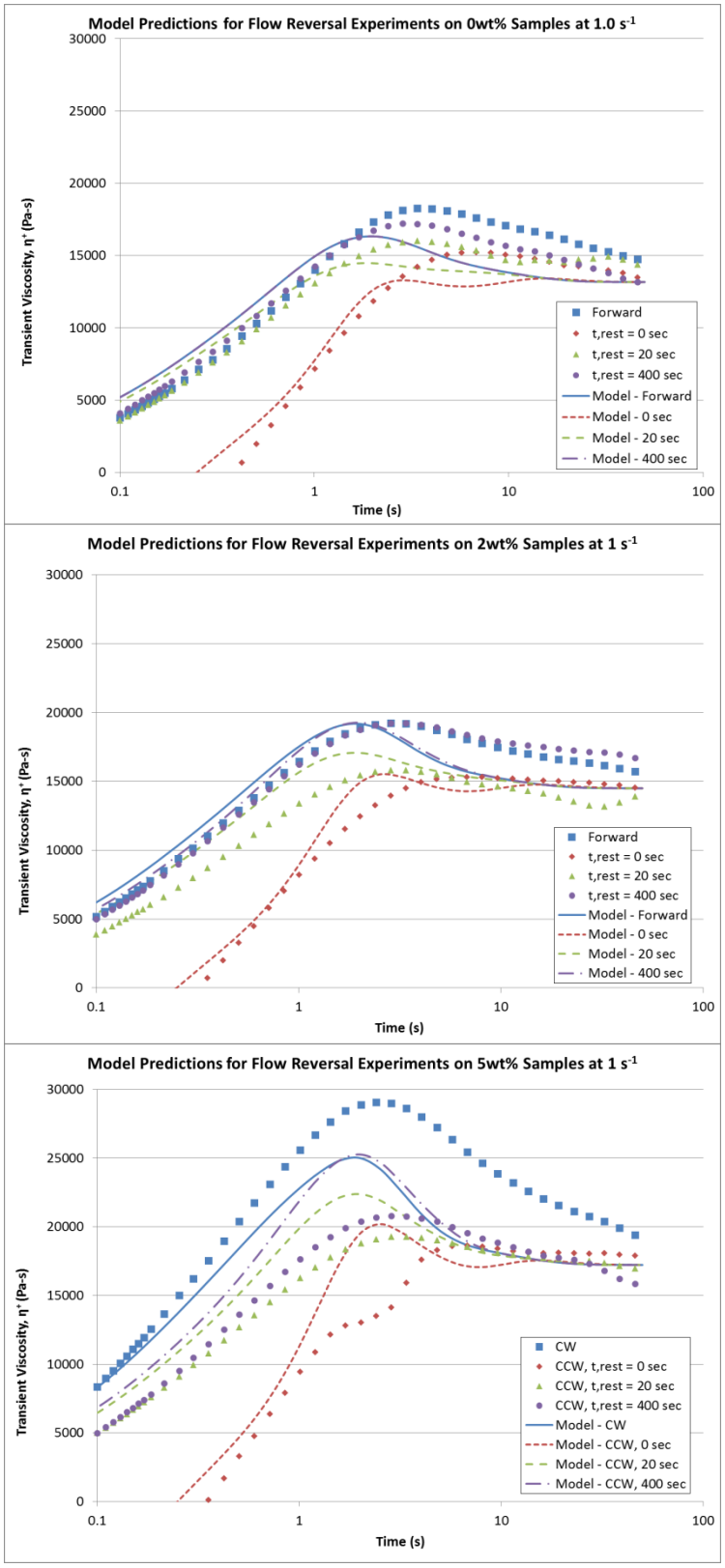

Figure 7: Transient Viscosity Response Curves during Flow Reversal at a Shear Rate of 1.0 s^{-1} for (a.) 0wt% (b.) 2wt%, and (c.) 5wt% Samples.

The transient viscosity curves for flow reversal studies performed at a CNF concentration of 5wt% are shown in Figure 8. Note that Figure 7c corresponds to the third graph in this data set. Also note that in these three figures, the axes are not the same.

In Figure 7b, the model predictions again do reasonably well to predict the qualitative trends and curve shapes, especially below the overshoot strain ($\gamma < 1$). The experimental variation is more pronounced in this figure, with the reverse viscosity curve at $t_{rest} = 0\ s$ rising above all other curves at steady state.

In Figure 7c, the same flow reversal trends that were seen previously at higher shear rates are no longer observed at this shear rate of $\dot{\gamma} = 0.01\ s^{-1}$. Instead, the transient viscosity rises like before at low strains, and seems to slightly plateau around a strain of $\gamma < 1$, but then continues to grow, eventually reaching a second plateau. In addition, the reverse viscosity curves corresponding to trials with nonzero rest times grew to steady shear viscosity values well above that seen for the forward direction.

Similar trends were observed for the same shear rate trials at 2wt% CNF concentration, but not quite as pronounced for 0wt% samples (neither shown here). These deviations from expected trends at the lowest shear rate suggests that a different behavior is taking place at the microstructural level. To give a constant strain of $\gamma = 50$, these trials at shear rates of $\dot{\gamma} = 0.01\ s^{-1}$ take place of a flow time of $t_{flow} = 5000\ s$ (about 1.4 hrs). It is possible that over this extended time period, polymer degradation takes place (explaining why the reverse viscosity is higher than the forward viscosity for the 0wt% samples, not shown). In addition, over these long time periods, the CNFs may aggregate to form a microstructure network, and the low shear rates may not provide

enough force to disentangle the aggregates. This might explain the observed gradual and monotonic increase in the transient viscosity during the flow period for the 5wt% samples.

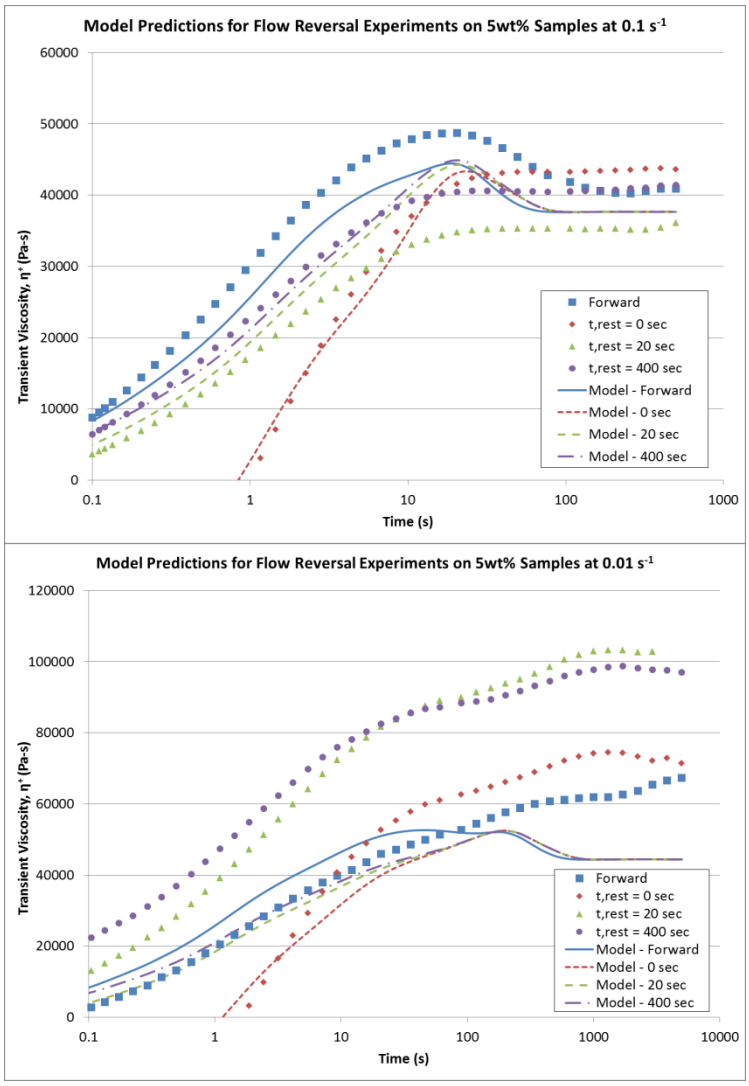

Figure 8: Transient Viscosity Response Curves during Flow Reversal for 5wt% Samples at Shear Rates of (a.) 0.1 s^{-1} (b.) and 0.01 s^{-1}.
(Note that the transient viscosity curves for the 5wt% samples sheared at a shear rate of 1.0 s^{-1} are shown in Figure 7c.)

The stress overshoot measurements from reverse flows at a shear rate of $\dot{\gamma} = 1.0\ s^{-1}$ are shown graphically in Figure 9. As seen from the graph, the stress overshoot generally increases at increasing rest times for the experimental results, matching the

model predictions. The model predicts that at rest times above approximately $t_{rest} = 70\ s$, very little increase in the stress overshoot will be observed, suggesting this is the rest time at which the composite is essentially completely relaxed. The model also predicts that the stress overshoot should increase at increasing CNF loadings, although this trend is not exhibited clearly in the experimental results. The fact that CNF weight percent has a less significant effect during reverse flows may be explained by the initial state of CNF orientation in the sample. Forward flows begin with CNFs in the randomly-oriented state, while reverse flows begin with the CNFs already oriented in the direction of flow. Thus, it is likely that the magnitude of the stress overshoot is dependent on the initial orientation of CNFs – a more random initial orientation results in a larger stress overshoot. This assertion is supported by the fact that the magnitudes of the stress overshoot were significantly lower for reverse flows with rest times of $t_{rest} = 400\ s$ than for their forward counterparts. Also, it is likely that the effect of CNF loading is more pronounced for initially randomly oriented samples than for initially flow-oriented samples.

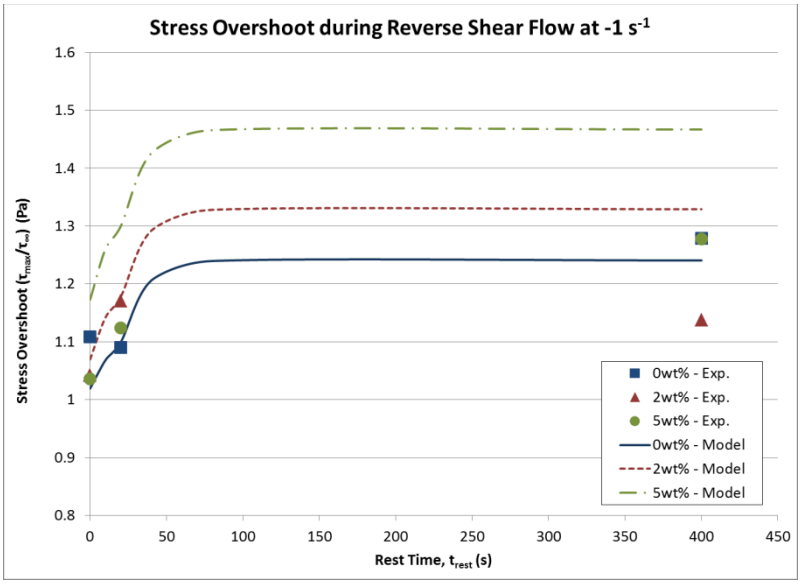

Figure 9: Stress Overshoot versus Rest Time during Transient Reverse Shear Experiments.

Figure 10 displays the transient first normal stress difference, $N1^+$, for flow reversal studies performed at a shear rate of $\dot{\gamma} = 1.0\ s^{-1}$. Note that the scales among the three graphs are identical for ease of comparison.

It is expected that the first normal stress difference would increase, exhibit a slight extended overshoot, and then decrease slightly to a steady shear value. This general curve shape can be observed in Figure 10. The model predictions match the experimental results reasonably well, although it is clear that the experimental variation is very high for the first normal stress difference. The first normal stress difference curve is slightly different for the reverse trial at a rest time of $t_{rest} = 0\ s$, since initially the normal force is already at a steady state value for this trial. For this curve, the normal stress decreases to a minimum near a strain of approximately $\gamma = 1$, and then increases back to its steady state value. This curve shape was observed experimentally, and validated with model predictions.

The experimental variation in the first normal stres difference measurements make even qualitative trends difficult to characterize. However, even from this scattered data set, it can be seen that the overshoot of $N1^+$ and its steady state values increase at increasing CNF loadings. In addition, as rest time increases, the reverse $N1^+$ curve matches more closely to the forward curve, a trend similar to that seen for transient viscosity results, again displaying that relaxation of the polymer structure has taken place.

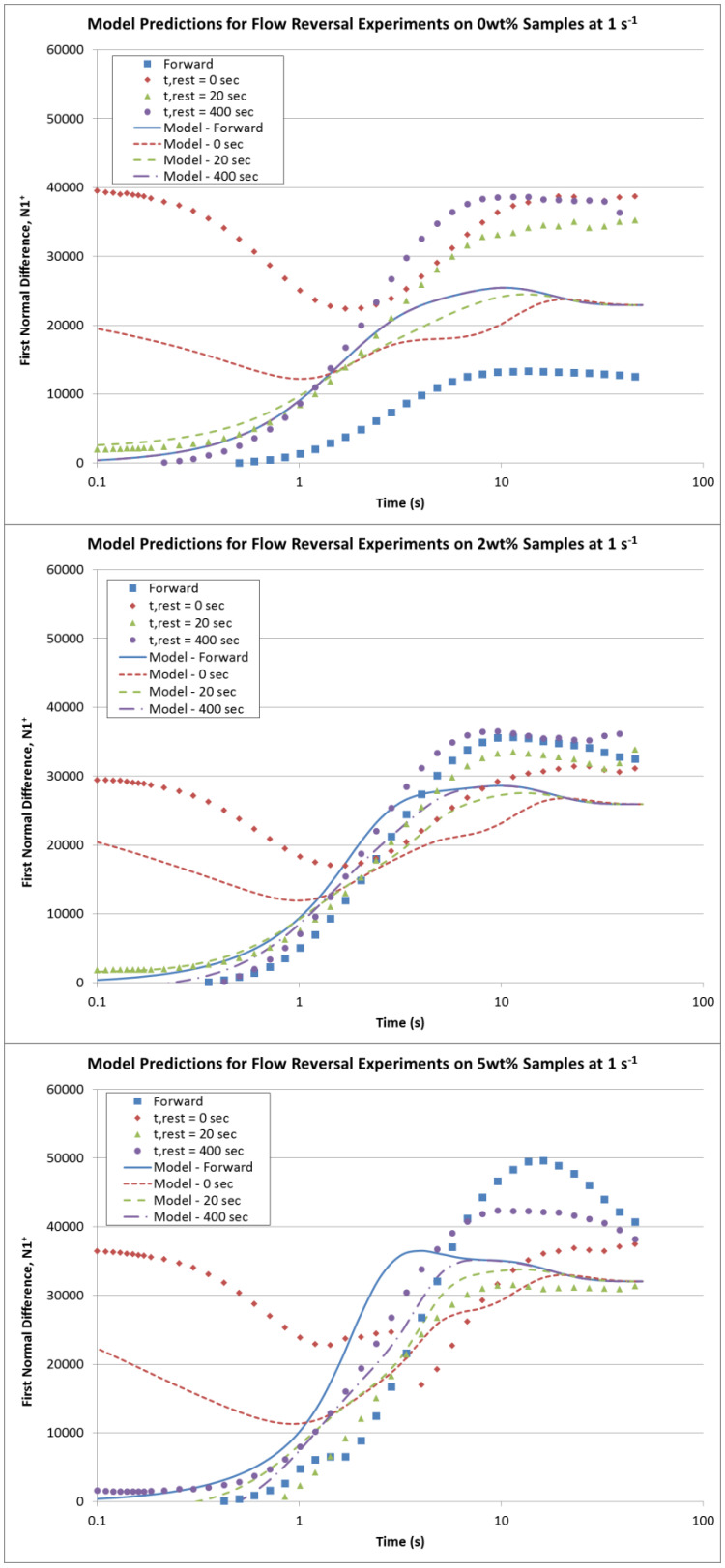

Figure 10: Transient First Normal Stress Difference during Flow Reversal at a Shear Rate of 1.0 s^{-1} for (a.) 0wt% (b.) 2wt%, and (c.) 5wt% Samples.

The results from the flow reversal studies give information on the effect of initial polymer stress and CNF orientation on the subsequent flow behavior. These rheological measurements can also help to elucidate the microstructural behavior that is taking place within the polymer matrix. For example, based on the results of this experiment, it can be inferred that the polymer relaxes and reconstitutes itself during periods of rest around non-Brownian and non-reorienting CNFs. This is supported by the observations that initial polymer stress has a large effect on the stress overshoot during flow reversals, but CNF weight percent does not. The unexpected phenomena observed at low shear rates and long shear times (Figure 8b) may also be explained by microstructural behavior, as discussed previously.

The experimentally observed behavior that deviated from model predictions may be explained by modifications to the model. The model presented here simplified interactions between CNFs and other CNFs and between CNFs and the polymer. To better describe the real behavior of the composites, it is necessary to investigate the effects of changing the values for the particle-particle interaction parameter (represented by C_I), and the polymer-particle interaction parameter (represented by σ).\

Conclusions and Future Work

This study investigated the effects of CNF loading, shear rate, and rest time on the rheological behavior of PS/CNF composites during flow reversal experiments. The effect of CNF loading and shear rate was also investigated on PS/CNF composites undergoing small amplitude oscillatory and steady shear flows. These experiments showed that the addition of nanofibers to a polymer matrix significantly affects the flow

behavior of the composite. For samples with initially random orientation, the addition of CNF particles increased both the stress overshoot and transient viscosity that was observed during flow. For samples with a flow-aligned orientation, increased CNF loadings again resulted in increased transient viscosity measurements, but any effect of CNF loading on the stress overshoot was not evident. This suggests that the magnitude of the stress overshoot is partially dependent on the pre-orientation and subsequent orientation evolution of CNFs during the flow period. The flow behavior was also strongly dependent on the initial polymer stress, dictated by the amount of rest time that was allowed for between flows. As the rest time increased in flow reversal experiments, the polymer matrix was allowed more time to relax and reform its structure, and the subsequent flow behavior more so resembled that of the initial flow behavior. As the rest time decreased, the observed stress overshoot during the reverse flow was significantly reduced, suggesting that the initial polymer stress also plays a role in the magnitude of the stress overshoot.

It is believed that the CNFs are weakly aggregated within the polymer matrix, but that higher shear rates overcome these particle-particle interactions, resulting in the orientation of individual nanofibers. Flows with low shear rates ($\dot{\gamma} = 0.01\ s^{-1}$) may actually result in the network build-up or agglomeration of fibers, resulting in significantly higher viscosities. Finally, based on the results it is believed that no significant fiber reorientation takes place during the rest time periods used in these flow reversal experiments. These interpretations of the microscopic behavior of the polymer composite are based on the macroscale rheological measurements only. The

quantification of CNF orientation during or following flows is suggested for future work in this area of study.

The experimental results were compared against the model prediction of a constitutive model presented in this study. Specifically, the model predictions for the transient viscosity and the first normal difference were validated against experimental results. The model predictions matched the experimentally observed qualitative trends well and the quantitative values with reasonable accuracy. The limitations in this model are currently in its inability to fully predict the effects of the particle-particle interactions (represented by the fitting parameter, C_I), and the polymer-particle interactions (represented by σ). Further investigation into the effect of these parameters, and how they can be accurately fitted to experimental results, is suggested for future work.

References

Advani, S.G. and Tucker, C.L. III. "The use of tensors to describe and predict fiber orientation in short fiber composites." J. Rheol., 31, (1987), 751-784.

Azaiez, J. "Constitutive equations for fiber suspensions in viscoelastic media." J. Non-Newtonian Fluid Mech., 66, (1996): 35-54.

Biercuk, M.J.; Llaguno, M.C.; Radosavljevic, M.; Hyun, J.K.; Johnson, A.T.; and Fischer, J.E. "Carbon nanotube composites for thermal management." Appl. Phys. Lett., 80, (2002): 2767-2769.

Bird, R.B.; Curtiss, C.F.; Armstrong, R.C.; and Hassager, O. *Dynamics of Polymeric Liquids.* Wiley, New York, (1987).

Caldiera, G.; Maia, J.M.; Carneiro, O.S.; Covas, J.A.; and Bernardo, C.A. "Production and characterization of innovative carbon fiber-polycarbonate composites." Polym. Compos., 19, (1998): 147-151.

Carneiro, O. S.; Covas, J.A.; Bernardo, C.A.; Caldeira, G.; Van Hattum, F.W.J.; Ting, J.-M.; Alig, R.L.; Lake, M.L. "Production and assessment of polycarbonate composites reinforced with vapour-grown carbon fibres," Compos. Sci. Technol., 58, (1998): 401–407.

Carneiro, O. S. and Maia, J.M. "Rheological behavior of _short_ carbon fiber/thermoplastic composites. Part I: The influence of fiber type, processing conditions and level of incorporation," Polym. Compos., 21, (2000): 960–969.

Ceccia, S.; Ferri, D.; Tabuani, D.; and Maffettone, P.L. "Rheology of carbon nanofiber-reinforced polypropylene." Rheol. Acta, 47, (2008): 425-433.

Choi, E.S.; Brooks, J.S.; Eaton, D.L.; Al-Haik, M.S.; Hussaini, M.Y.; Garmestani, H.; Li, D.; and Dahmen, K. "Enhancement of thermal and electrical properties of carbon nanotube polymer composites by magnetic field processing." J. Appl. Phys., 94, (2003): 6034-6039.

Cipriano, B.H.; Kota, A.K.; Gershon, A.L.; Laskowski, C.J.; Kashiwagi, T.; Bruck, H.A.; and Raghavan, S.R. "Conductivity enhancement of carbon nanotube and nanofiber-based polymer nanocomposites by melt annealing." Polymer, 49, (2008): 4846-4851.

Cooper, C.A.; Ravich, D.; Lips, D.; Mayer, J.; and Wagner, H.D. "Distribution and alignment of carbon nanotubes and nanofibrils in a polymer matrix." Compos. Sci. Technol, 62, (2002): 1105-1112.

Dinh, S.M. and Armstrong, R.C. "A rheological equation of state for semiconcentrated fiber suspensions." J. Rheol., 28, (1984): 207-227.

Du, F.; Guthy, C.; Kashiwagi, T.; Fischer, J.E.; Winey, K.I. "An infiltration method for preparing single-wall nanotube/epoxy composites with improved thermal conductivity." J. Polym. Sci., Part B: Polym. Phsy., 44, (2006): 1513-1519.

Dyke, C.A. and Tour, J.M. "Covalent functionalization of single-walled carbon nanotubes for materials applications." J. Phys. Chem. A, 108, (2004): 11151-11159.

Eslami, H.; Grmela, M.; Bousmina, M. "Structure build-up at rest in polymer nanocomposites: flow reversal experiments." Journ. of Polym. Sci.: Part B: Polym. Phys., 47, (2009): 1728-1741.

Geng, H.; Rosen, R.; Zheng, B.; Shimoda, H.; Fleming, L.; Liu, J.; and Zhou, O. "Fabrication and properties of composites of poly(ethylene oxide) and functionalized carbon nanotubes." Adv. Mater., 14, (2002): 1387-1390.

Glasgow, D.G.; Tibbetts, G.G.; Matuszewski, M.J.; Walters, K.R.; and Lake, M.L. *Proceedings of the 49th International SAMPE Symposium and Exhibition.* Society for the Advancement of Material and Process Engineering, Covina, CA, (2004): 2355-2364.

Hammel, E.; Tang, X.; Trampert, M.; Schmitt, T.; Mauthner, K.; Eder, A.; and Potschke, P. "Carbon nanofibers for composite applications." Carbon, 42, (2004): 1153-1158.

Higgins, B.A. and Brittain, W.J. "Polycarbonate carbon nanofiber composites." Eur. Polym. J., 41, (2005): 889-893.

Iijima, S. "Helical microtubules of graphitic carbon." Nature, 354, (1991): 56-58.

Jaing, X.; Bin, Y.; and Matsuo, M. "Electrical and mechanical properties of polyimide-carbon nanotubes composites fabricated by in situ polymerization." Polymer, 46, (2005): 7418-7424.

Kagarise, C.; Koelling, K.W.; Wang, Y.; and Bechtel, S.E. "A unified model for polystyrene-nanorod and polystyrene-nanoplatelet melt composites." Rheol. Acta, 47, (2008): 1061-1076.

Kagarise, C.D. "Rheological characterization and modeling of micro- and nano-scale particle suspensions." Dissertation, The Ohio State University, (2009).

Kagarise, C.; Xu, J.; Wang, Y.; Mahboob, M.; Koelling, K.W.; and Bechtel, S.E. "Transient shear rheology of carbon nanofiber/polystyrene melt composites." J. Non-Newtonian Fluid Mech., 165, (2010): 98–109.

Kagarise, C.; Miyazono, K.; Mahboob, M.; Koelling, K.W.; and Bechtel, S.E. "A constitutive model for characterization of shear and extensional rheology and flow

induced orientation of carbon nanofiber/polystyrene melt composites." J. Rheol., 55(4), (2011): 781-807.

Kumar, S.; Doshi, H.; Srinivasarao, M.; Park, J.O.; and Schiraldi, D.A. "Fibers from polypropylene/nano carbon composites." Polymer, 43, (2002): 1701–1703.

Lake, M.L.; Glasgow, D.G.; Kwag, C.; and Burton, D.J. *Proceedings of the 47th International SAMPE Symposium and Exhibition.* Society for the Advancement of Material and Process Engineering, Covina, CA, (2002): 1794–1800.

Letwimolnun, W.; Vergnes, B.; Ausias, G.; and Carreau, P.J. "Stress overshoots of organoclay nanocomposites in transient shear flow." J. Non-Newtonian Fluid Mech., 141, (2007): 167-179.

Lozano, K. and Barrera, E.V. "Nanofiber-reinforced thermoplastic composites. I. Thermoanalytical and mechanical analyses." J. Appl. Polym. Sci., 79, (2001): 125–133.

Lozano, K.; Bonilla-Rios, J.; and Barrera, E.V. "A study on nanofiber-reinforced thermoplastic composites (II): Investigation of the mixing rheology and conduction properties." J. Appl. Polym. Sci., 80, (2001): 1162–1172.

Lozano, K.; Yang, S.; and Zeng, Q. "Rheological analysis of vapor-grown carbon nanofiber-reinforced polyethylene composites." J. Appl. Polym. Sci., 93, (2004): 155-162.

Ma, H.; Zeng, J.; Realff, M.L.; Kumar, S.; and Schiraldi, D.A. "Processing, structure, and properties of fibers from polyester/carbon nanofiber composites." Compos. Sci. Technol., 63, (2003): 1617-1628.

Meincke, O.; Kaempfer, D.; Weickmann, H.; Friedrich, C.; Vathauer, M.; and Warth, H. "Mechanical and electrical conductivity of carbon-nanotube filled polyamide-6 and its blends with acrylonitrile/butadiene/styrene." Polymer, 45, (2004): 739-748.

Miyazono, K.; Kagarise, C.D.; Koelling, K.W.; Mahboob, M.; and Bechtel, S.E. "Shear and extensional rheology and flow-induced orientation of carbon nanofiber/polystyrene melt composites." Journ. Of Appl. Polym. Sci., 119, (2011): 1940-1951.

Ramasubramaniam, R.; Chen, J.; and Liu, H. "Homogeneous carbon nanotube/polymer composites for electrical applications." Appl. Phys. Lett., 83, (2003): 739-748.

Solomon, M.J.; Almusallam, A.S.; Seefeldt, K.F.; Somwangthanaroj, A.; and Varadan, P. "Rheology of polypropylene/clay hybrid materials." Macromolecules, 34, (2001): 1864-1872.

Shaqfeh, E.S. and Fredrickson, G.H. "The hydrodynamic stress in a suspension of rods." Phys. Fluids A, 2, (1990): 7-24.

Tibbets, G.G. and McHugh, J.J. "Mechanical properties of vapor-grown carbon fiber composites with thermoplastic matrices." J. Mater. Res., 14, (1999): 2871-2880.

Tucker, C.L. III. "Flow regimes for fiber suspensions in narrow gaps." J. Non-Newtonian Fluid Mech., 39, (1991): 239-268.

Van Hattum, F.W.J.; Bernardo, C.A.; Finegan, J.C.; Tibbetts, G.G.; Alig, R.L.; Lake, M.L. "A study of the thermomechanical properties of carbon fiber-polypropylene composites." Polym. Compos., 20, (1999): 683-688.

Wang, Y.; Xu, J.; Bechtel, S.E.; and Koelling, K.W. "Melt shear rheology of carbon nanofiber/polystyrene composites," Rheol. Acta, 45, (2006): 919–941.

Xu, J.; Chatterjee, S.; Koelling, K.W.; Wang, Y.; and Bechtel, S.E. "Shear and extensional rheology of carbon nanofiber suspensions." Rheol. Acta, 44, (2005): 537-562.

Yang, S.; Lozano, K.; Lomeli, A.; Foltz, H.D.; and Jones, R. "Electromagnetic interference shielding effectiveness of carbon nanofiber/LCP composites." Composites, Part A, 36, (2005): 691-697.

Zeng, J.; Saltysiak, B.; Johnson, W.S.; Schirali, D.A.; and Kumar, S. "Processing and properties of poly(methyl methacrylate)/carbon nano fiber composites." Composites, Part B, 35, (2004): 173-178.